Journal of Hazardous Materials 396 (2020) 122691

Contents lists available at ScienceDirect

Journal of Hazardous Materials

journal homepage: www.elsevier.com/locate/jhazmat

Comparison of the colloidal stability, mobility, and performance of nanoscale zerovalent iron and sulfidated derivatives

Yiming Su[a], David Jassby[a], Yalei Zhang[b], Arturo A. Keller[c], Adeyemi S. Adeleye[d,*]

[a] Department of Civil and Environmental Engineering, University of California, Los Angeles, CA 90095, USA
[b] State Key Laboratory of Pollution Control and Resources Reuse, Key Laboratory of Yangtze Water Environment for Ministry of Education, Tongji University, Shanghai 200092, China
[c] Bren School of Environmental Science & Management, University of California, Santa Barbara and University of California Center for Environmental Implications of Nanotechnology, Santa Barbara, California, CA 93106, USA
[d] Department of Civil and Environmental Engineering, University of California, Irvine, CA 92697-2175, USA

GRAPHICAL ABSTRACT

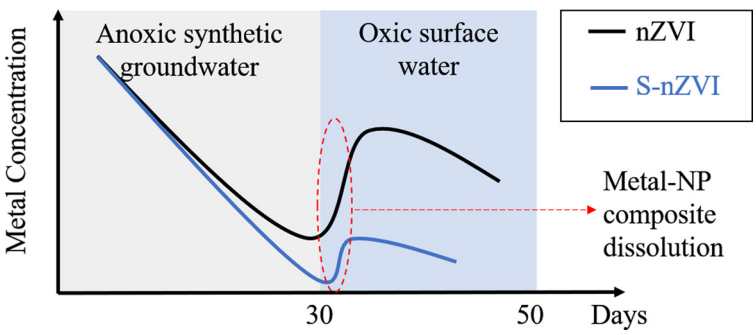

ARTICLE INFO

Editor: Daniel CW. Tsang

Keywords:
nZVI
Nanoremediation
Colloidal stability
Particle transport
Metal sequestration

ABSTRACT

Nanoscale zerovalent iron (nZVI) and sulfidated nanoscale zerovalent iron (S-nZVI) have been increasingly studied for heavy metal removal in the subsurface. However, a comprehensive comparison of the effectiveness of the technologies and the stability of derived metal-adsorbed composites is lacking. In this study, we evaluated the colloidal stability and transport of nZVI, S-nZVI and S-nZVI modified with nanosized silica (FeSSi). Furthermore, we monitored the metal immobilization performance of the three nanoparticles (NPs) under anoxic conditions in synthetic groundwater for 30 days. The NP-metal composites were thereafter discharged into a river water and metal remobilization was monitored for 20 days. Sulfidation improved the colloidal stability of nZVI in both simple media and in natural waters, although a lower initial agglomeration rate constant (k_a) was observed in unmodified nZVI at acidic pH. The transport of nZVI in saturated soil column was enhanced with sulfidation due to decreased electrostatic attraction between the NPs and sand. The three NPs sequestered more than 80 % of Cu^{2+}, Zn^{2+}, Cd^{2+} and $Cr_2O_7^{2-}$ from groundwater. Among the three NPs tested, S-nZVI had a slightly higher removal capacity for metals than nZVI in synthetic groundwater and the chemical stability of metal-S-nZVI composites upon discharge into river water was the highest.

* Corresponding author.
E-mail address: adeyemi.adeleye@uci.edu (A.S. Adeleye).

https://doi.org/10.1016/j.jhazmat.2020.122691
Received 31 December 2019; Received in revised form 7 April 2020; Accepted 8 April 2020
Available online 14 April 2020
0304-3894/ © 2020 Elsevier B.V. All rights reserved.

1. Introduction

Nanoscale zerovalent iron (nZVI) has long been regarded as an effective nanoparticle (NP) for in situ treatment of a wide variety of contaminants in soil, groundwater and wastewater, particularly chlorinated organic compounds (Su et al., 2014a; Adeleye et al., 2016a; Zhang et al., 2013a; Su et al., 2014b; Qian et al., 2018; Li et al., 2008; Liu and Lowry, 2006; Liu et al., 2007). For instance, more than 90 % reduction of perchloroethylene (PCE) was reported within a month of injecting a mixture of stabilized nZVI and micron-sized zerovalent iron into a contaminated site at Bornheim, Germany (Mueller et al., 2012). The challenges associated with nZVI-based remediation include limited mobility in the subsurface (arising from agglomeration), poor removal efficiency for certain target pollutants (e.g. cadmium), and rapid passivation of particles in the environment, which affects their performance (He et al., 2010; Zhang, 2003; Li et al., 2016). In the last two decades, research has focused on improving the (1) stability of nZVI by supporting it on porous materials (like bentonite, kaolinite, and activated carbon) Shi et al., 2011; Yu et al., 2018; Mackenzie et al., 2012; Chang et al., 2010; Bello et al., 2019) or polymers (Jiemvarangkul et al., 2011; Liu et al., 2016; Raychoudhury et al., 2010), and (2) performance by doping nZVI with catalytic metals (such as palladium, copper, and gold) (Su et al., 2014b; Kadu and Chikate, 2013; Chen et al., 2011; Shi et al., 2019). The side reaction of nZVI with water remained a major drawback of the technology until the more recent development of sulfidated nZVI (S-nZVI) (Fan et al., 2017a; Su et al., 2015a; Song et al., 2017a; Su et al., 2016a; Fan et al., 2016, 2017b; Qin et al., 2017). Xu et al. reported that a low degree of sulfidation (0.02–0.65 mol % S/Fe) inhibited the reaction of nZVI with water (up to 13-fold), and enhanced its reactivity with trichloroethene (up to 14-fold) and electron efficiency (up to 20-fold) (Xu et al., 2019a, 2020; Xu et al., 2019b). A recent field study further demonstrated that S-nZVI can effectively reduce chlorinated solvents in the subsurface with no observable accumulation of shorter-chain chlorinated volatile organics (Nunez Garcia et al., 2020).

However, unlike organic pollutants, which can be removed by adsorption and/or degradation (Xiang et al., 2020, 2019; Tang et al., 2016), heavy metals in the subsurface can only be immobilized (Bello et al., 2019). While sulfidation increased the removal capacity of nZVI for cadmium and chromate from 40 to 85 mg/g (Su et al., 2015a) and 2.5–25 mg/g (Shao et al., 2018), respectively, the efficacy of nZVI/S-nZVI for metals remediation in the subsurface has not been comprehensively evaluated. The removal of metals by nZVI/S-nZVI requires contact between NPs and metals, which implies that high NP colloidal stability and mobility are desirable.

In a previous study we found that S-nZVI was more stable than nZVI in the presence of some common ions (Song et al., 2017b); but till date, the impact of pH, different water matrixes, and the extent of sulfidation on the aggregation and mobility of nZVI is still unknown. More so, metals are immobilized by nZVI/S-nZVI via different mechanism, including adsorption, co-precipitation, and reduction (Zhang et al., 2013a). For instance, Ag^+ and Cu^{2+} were mainly reduced onto NP surface, while Zn^{2+} was primarily removed by adsorption and co-precipitation (Ling et al., 2018, 2017). Therefore, the chemical stability of the metal-NP composites formed after immobilization will vary from one metal to another. The decision to substitute S-nZVI for pristine nZVI in metal remediation should be informed by (1) the relative removal performance for the target metal(s), and (2) the tendency for the sequestered metal to be remobilized from the metal-NP composite in the long term. The scientific data required for such holistic considerations are currently lacking.

The goals of this study were to (1) comparatively study the colloidal stability and transport of nZVI, S-nZVI (S/Fe molar ratio = 0.28), and nano silica infused sulfidated nZVI (named, FeSSi, S/Fe molar ratio = 0.48); (2) compare the removal capacity of the three NPs for different heavy metals in groundwater; and (3) compare the chemical stability of the generated metal-NP composites after discharge from groundwater into river water.

2. Materials and methods

2.1. Chemicals

Analytical grade sodium borohydride ($NaBH_4$, 98 %), dithionite ($Na_2S_2O_4$), ferric chloride anhydrous ($FeCl_3$), sodium hydroxide (NaOH), hydrochloric acid (HCl), sodium chloride (NaCl), sodium sulfate (Na_2SO_4) potassium sulfate (K_2SO_4), sodium bicarbonate ($NaHCO_3$), calcium chloride ($CaCl_2$), magnesium chloride ($MgCl_2$), cadmium acetate ($Cd(CH_3COO)_2$), copper chloride ($CuCl_2$), potassium dichromate ($K_2Cr_2O_7$), ammonium dimolybdate ($(NH_4)_2Mo_2O_7$) were purchased from Sigma-Aldrich (Shanghai, China & MO, USA). Nano-SiO_2 (100 nm) were obtained from Beijing DK Nanotechnology Co. Ltd.

2.2. Nanoparticles

S-nZVI was prepared as described by Su et al. (2015b, 2018a). Briefly, 7.6 g $NaBH_4$ and 1 g of $Na_2S_2O_4$ were titrated into 4.9 g $FeCl_3$ solution (titration rate ~1 L/h), making a nominal S/Fe molar ratio of 0.28. Pristine nZVI was prepared in a similar manner but without the addition of $Na_2S_2O_4$. FeSSi was prepared similar to S-nZVI but the $NaBH_4/Na_2S_2O_4$ solution was seeded with nano-SiO_2 prior to titration into the $FeCl_3$ solution (Su et al., 2016a). The major physicochemical properties of the three particles used in this study have been published previously (Su et al., 2016a, 2015b, 2018a). The average particle size of nZVI is about 60 nm, while that of S-nZVI and FeSSi are about 100 nm and 200 nm, respectively (Fig. 1). The particles of nZVI and S-nZVI formed fractal, chain-like clusters but similar chain-like structures are not present in FeSSi. About 13.7 % of the total Fe in S-nZVI exists as FeS in the shell while the shell of nZVI is composed of iron hydroxides (Zhang et al., 2013b; Mangayayam et al., 2019). The FeS content of the shell is about 24.2 % in FeSSi. The Fe° content of nZVI, S-nZVI, and FeSSi are 83.5 %, 90.8 %, and 55.6 %, respectively (Su et al., 2016a). The different composition of these three NPs results in different isoelectric points (IEP). The IEP for nZVI, S-nZVI, and FeSSi is pH 7.5, pH 5, and pH 5.5, respectively (Su et al., 2016a; 2015b; 2018a).

2.3. Natural waters, wastewater and stock solutions

Agglomeration kinetics of the NPs was studied in simple media (that is, aqueous solutions of a salt) and different complex aqueous media present in the environment. To test the effect of different environmentally relevant anions on NPs' colloidal stability, 50 mM stock solutions of different sodium salts (NaCl, $NaNO_3$, Na_2SO_4, and Na_2CO_3) were prepared. In addition, a 50 mM stock solution of $CaCl_2$ was prepared, to test the effect of cation valency (Na^+ and Ca^{2+}). Stocks of buffer (pH 5 = acetate, pH 7 = phosphate, and pH 9.3 = carbonate) were prepared to test the effect of pH on colloidal stability. In addition, colloidal stability experiments were conducted in natural waters and wastewater. Seawater was collected from UCSB's Marine Science Institute ocean water line, which is pumped through a sand filter from an offshore inlet (located in the Pacific Ocean in Santa Barbara, CA). Wastewater was collected from the secondary effluent of El Estero Wastewater Treatment Plant (Santa Barbara, CA). Groundwater was obtained from a monitoring well in Santa Barbara, CA, and river water was collected from Upper Middle Creek in Malibu, CA. The characterization of all these waters have been presented in previous studies (Conway et al., 2015; Roehrdanz et al., 2017). All the waters were passed through 0.1 μm filters (Millipore, Ireland) and stored at 4 °C prior to colloidal stability experiments.

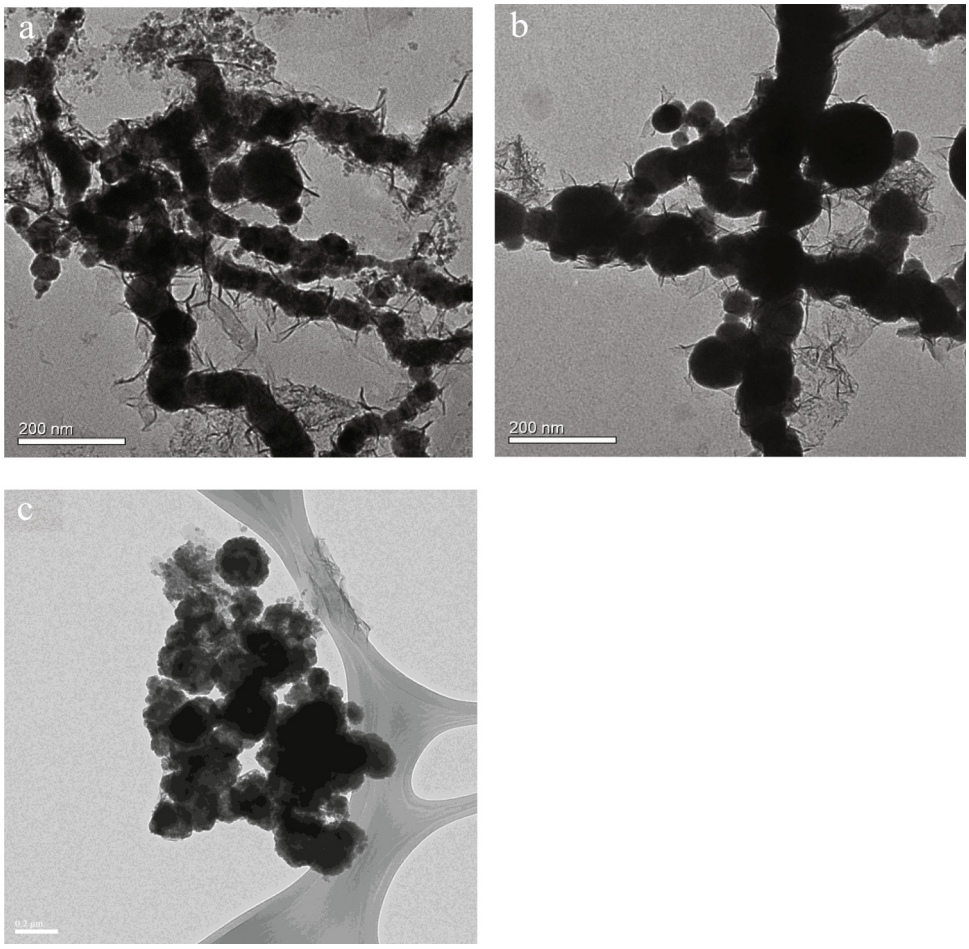

Fig. 1. Transmission electron micrographs of (a) nZVI, (b) S-nZVI, and (c) FeSSi. Each scale bar is 200 nm.

2.4. Colloidal stability experiments

The colloidal stability of NPs in natural waters and different salt solutions was investigated via time-resolved agglomeration kinetics studies (Adeleye et al., 2016b; Keller et al., 2010; Adeleye and Keller, 2016). NP stock suspensions were bath-sonicated (Branson 2510) for 30 min to disperse the particles. Measured aliquots of NP stock suspensions, salt (NaCl, $NaNO_3$, Na_2SO_4, Na_2CO_3, or $CaCl_2$), and buffer were pipetted into a cuvette, and diluted with deionized (DI) water (Barnstead NANOpure Diamond, 18.2 MΩ-cm). The final concentration of NP, salt and buffer for each treatment was 50 mg/L, 10 mM, and 5 mM, respectively. Effect of pH on particle stability was studied in DI water and 10 mM NaCl using 5 mM of the pH 5, 7, and 9.3 buffers. After adding all the stocks in a cuvette, they were mixed for 5 s with a Misonix Sonicator S-4000 (QSonica LLC). For studies in natural waters, the final NP concentration was also 50 mg/L, with no further addition of salt and buffer. Agglomeration was studied at 20 °C via dynamic light scattering (DLS) using a Zetasizer Nano-ZS90 (Malvern, UK). The intensity weighted hydrodynamic diameter (D_h) of NPs was measured at 30 s intervals for a minimum of 60 min. The initial agglomeration rate constants (k_a) of the NPs reflects doublet formation, and are proportional to the initial rate of increase of D_h(t) with time (t), and the inverse of initial number concentration of the NPs, N_0, (Eq. 1) (Wang et al., 2018; Chowdhury et al., 2015):

$$k_a \propto \frac{1}{N_0}\left[\frac{dD_h(t)}{dt}\right]_{t\to 0} \tag{1}$$

k_a was obtained from the slope of the best fit line of $\left[\frac{dD_h(t)}{dt}\right]_{t\to 0}$. The analysis requires that the final D_h(t) be approximately 1.3 of initial D_h, where sufficient doublets and a few higher-order aggregates have formed. For this study we used D_h(t) = 1.25 × initial D_h to determine each k_a. In the few cases where agglomeration was extremely slow, the regression analysis was performed with data obtained over a long time (Chen and Elimelech, 2007).

2.5. Nanoparticle transport

For below-ground remediation, nZVI is directly injected into the subsurface (Mueller et al., 2012). Thus, the efficacy of nZVI-based remediation in the subsurface largely depends on the mobility of NPs. Therefore, it is important to compare the mobility of the three NPs. Nanoparticle transport was studied in sand column (radius = 1 cm; height = 9 cm). The column was filled with washed quartz sand (45 µm grain size). The sand was washed three times with 2% v/v HNO_3, and six times with DI water thereafter. To avoid possible interferences from unknown substances in natural groundwater, a synthetic groundwater was used for the transport study. The synthetic groundwater was composed of NH_4Cl (1 mM), $MgCl_2$ (0.05 mM), $MnCl_2$ (0.02 mM), NaCl (0.12 mM), $CaCl_2$ (6 mM), $Na_2HPO_4{\cdot}2H_2O$ (0.45 mM), KH_2PO_4 (0.15 mM), Na_2SO_4 (1 mM), and $NaHCO_3$ (1 mM) (Middeldorp et al., 1998). The initial pH of groundwater was set at 6.5. Preliminary column transport studies were performed using NaCl as the tracer to determine the sand porosity/pore volume (PV). Chloride ion (Cl^-) concentration in the effluent was measured by ion chromatography (ICS-5000, Thermo Fisher, Waltham, MA). Before the addition of NP or tracer, the packed saturated sand column was equilibrated by pumping 20 PVs of synthetic groundwater using a peristaltic pump (2.1 cm^3/hr, which is a typical groundwater flow rate) (Song et al., 2017a). For the

studies, 0.1 g of NP was added into the top interspace of column while synthetic groundwater continued to be pumped through the column for 51 PVs. Effluent was collected at 1.5 PVs intervals. At the end of the experiment, 5 mL of collected effluent was digested with 5% HNO_3 and analyzed via inductively coupled plasma-optical emission spectrometry (ICP-OES, Agilent 720ES, Japan). The columns, with the sand and retained particles, were frozen and cut into pieces (from top to the bottom: 2, 2, 2, and 3 cm, corresponding to Layer 1, 2, 3, and 4, respectively). The sand (with retained NPs) collected from each layer piece was digested with aqua regia at 110 °C for 2 h. The digestate was collected and diluted with 5% HNO_3 prior to ICP-OES analysis. Total Fe mass recovery was 90–95 % of the total Fe added into column. Fe mass (M_x, x = 1, 2, 3, 4) in each layer was normalized with total Fe mass recovered from the column ($M_{tot\text{-}in\text{-}col}$) as shown in Eq. 2:

$$R_x = \left(\frac{M_x}{M_{tot-in-col}}\right) \tag{2}$$

2.6. Remediation and chemical stability of metal-nanoparticle mixture

To compare the performance of the three NPs for metal sequestration, we studied the remediation of Cu^{2+}, Zn^{2+}, Cd^{2+} and $Cr_2O_7^{2-}$ via batch studies. Synthetic groundwater, spiked with 10 mg/L of each contaminant, was treated with 0.5 g/L of nZVI, S-nZVI, or FeSSi. The samples were placed on a shaker (250 rpm, 25 ± 1 °C, Shanghai Fengling Laboratory Instrument FLY-111B, China) throughout the study. The performance of each NP was determined by considering residual dissolved metal in synthetic groundwater after 30 d.

Further studies were conducted to determine the chemical stability of the metal-NP composite formed from the adsorption process, particularly if the composite discharges with groundwater into a nearby surface water. After 30 d of running the adsorption experiments in synthetic groundwater, the metal-NP composite was used to dose previously uncontaminated river water to achieve a final NP concentration of 0.167 g/L. The river water was collected from the confluence of the Suzhou River and Huangpu River (Shanghai, China) and its main characteristics (pH = 7.88; total organic carbon = 18.75 mg/L; conductivity = 216.40 μS/cm) were presented in our previous study (Su et al., 2018b). To determine chemical stability, the concentration of adsorbed metal and Fe ions in the dosed river water was monitored for 20 d via ICP-OES.

3. Results and discussions

3.1. Stability experiments in simple media

3.1.1. Effect of pH

Agglomeration of particles were investigated at acidic (pH 5), neutral (pH 7), and basic (pH 9.3) conditions in order to understand how different pH conditions affect the colloidal stability of the NPs in the environment. Of the three pH conditions, the slowest agglomeration was observed at neutral pH (pH 7) for the three particles, both in DI water and in 10 mM NaCl. In both media, S-nZVI had the lowest initial agglomeration rate constants (k_a) at pH 7 and 9.3, while nZVI had the lowest k_a at pH 5 (Fig. 2 and S1). At 10 mM, while the k_a for S-nZVI was 35.1 and 80.7 nm/min at pH 7.0 and 9.3, respectively, the k_a increased to 122.3 nm/min at pH 5. The k_a of FeSSi at 10 mM, which is also sulfidated, was even higher at pH 5 (k_a = 151.7 nm/min). Conversely, while nZVI had a k_a of 100.8 nm/min at pH 5 (10 mM NaCl), its k_a at pH 9.3 was two-fold that of S-nZVI (at the same pH) (k_a = 161.5 nm/min).

The agglomeration of nZVI is mainly caused by low electrostatic repulsion and magnetic attraction (O'Carroll et al., 2013). The poor colloidal stability of S-nZVI and FeSSi at pH 5 can be partially explained by the closeness of their IEP to this acidic pH. NPs have practically no surface charge at their IEP, which, as mentioned earlier, is pH 5 for S-nZVI and pH 5.5 for FeSSi. In contrast, the surface of nZVI is positively charged at pH 5 since its IEP is pH 7.5. Although nZVI will be negatively charged at pH 9.3, both sulfidated NPs are expected to be more strongly charged at the basic pH based on their IEPs. The NPs also dissolve faster at acidic conditions like in pH 5, which may further promote agglomeration due to electrical double layer screening by the released Fe^{2+}.

According to the Derjaguin-Landau-Verwey-Overbeek (DLVO) theory, the further the pH is away from the IEP of colloids, the higher the magnitude of the surface charge, favoring colloidal stability of the NPs via promoted electrostatic repulsion. However, we found that the three NPs mostly have lower k_a values at pH 7 compared to pH 9.3 (which is further away from their IEPs). Additional studies are needed to determine the exact reason for this behavior, but we hypothesize that it is due to more rapid surface modification by the abundant OH– present at pH 9.3. The modification may be leading to the formation of oxides of iron with much higher IEPs than the original NPs (for instance, the IEP of α-Fe_2O_3 is 7.8–9.2, and that of Fe_3O_4 is 8 (Lei et al., 2018)).

As for magnetic attraction, magnetic NP dispersions may undergo dipole − dipole attraction between the magnetic moments of individual particles, which may lead to agglomeration and reduced colloidal stability (Phenrat et al., 2007). we showed in our previous studies (Su et al., 2015a; Song et al., 2017b; Su et al., 2016b) that the magnetization (M) of FeSSi (M = 65.5 emu/g) and nZVI (60.8 emu/g) are much greater than that of S-nZVI (M = 2.25 emu/g). In addition, since the magnetic attraction of particles depends on the particle size to the sixth power (Adeleye et al., 2013; Phenrat et al., 2008), the larger size of FeSSi further enhances agglomeration. Additional efforts are needed to quantify the contribution of magnetization to the total interaction potential for each NP compared to the conventional forces typically accounted for in the classical DLVO theory.

Apart from electrostatic repulsion and strong magnetic attraction, NP agglomeration may also be impacted by particle size and density. Based on the DLVO theory, interaction potential increases as particle size increases (He et al., 2008). More so, the agglomeration rate of larger particles is slower due to slower diffusion and thus, particle-particle collision. It is difficult to make direct comparison between the obtained k_a and size of the three particles studied here since they are inherently chemically different. Although density plays some role in NP agglomeration and sedimentation, a previous study showed that particle density had minimal effects on the agglomeration of iron-based NPs compared to concentration, particle size, and magnetic attraction (Phenrat et al., 2007).

Assuming the three NPs have comparable remediation efficiencies for a target contaminant in aqueous media or groundwater, an important consideration for the choice of NP to use is the mobility of NPs in the media. As discussed earlier, mobility is decreased by NP agglomeration, which is influenced by media pH. The most appropriate NP has the lowest k_a at the relevant pH condition, and thus, the lowest tendency to be removed from the aqueous phase via agglomeration. Based on the results obtained at 10 mM NaCl (which is more representative of the real environment than DI water), nZVI may have a higher mobility than S-nZVI and FeSSi in the subsurface under slightly acidic environment, and may be the ideal NP under this condition (assuming no significant differences in remediation performance). Meanwhile, S-nZVI may be better for neutral and alkaline environments, based on its least tendency to agglomerate under these conditions.

3.1.2. Effect of ionic species

Na^+ and Ca^{2+} ions are present in groundwater in moderate amounts. They may be abundant in cases of seawater intrusion or when there is high amount of limestone in the subsurface. Here, we tested the impact of different common anions of Na-salts on the agglomeration kinetics of the three NPs at pH 7. In addition, a divalent salt, $CaCl_2$, was tested. The k_a of the three NPs was influenced by the different anions

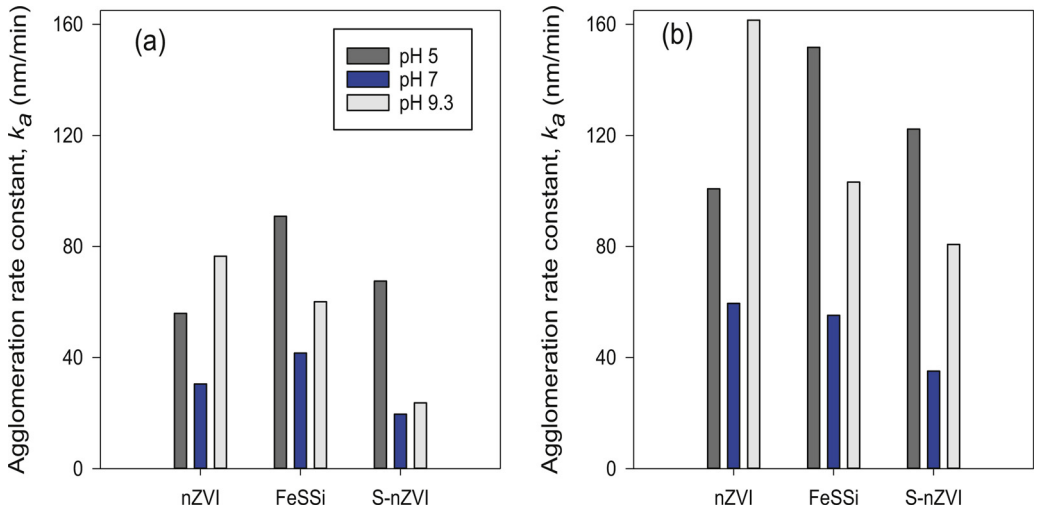

Fig. 2. The initial agglomeration rate constants (k_a) of nZVI, FeSSi, and S-nZVI in (a) DI water and (b) 10 mM NaCl.

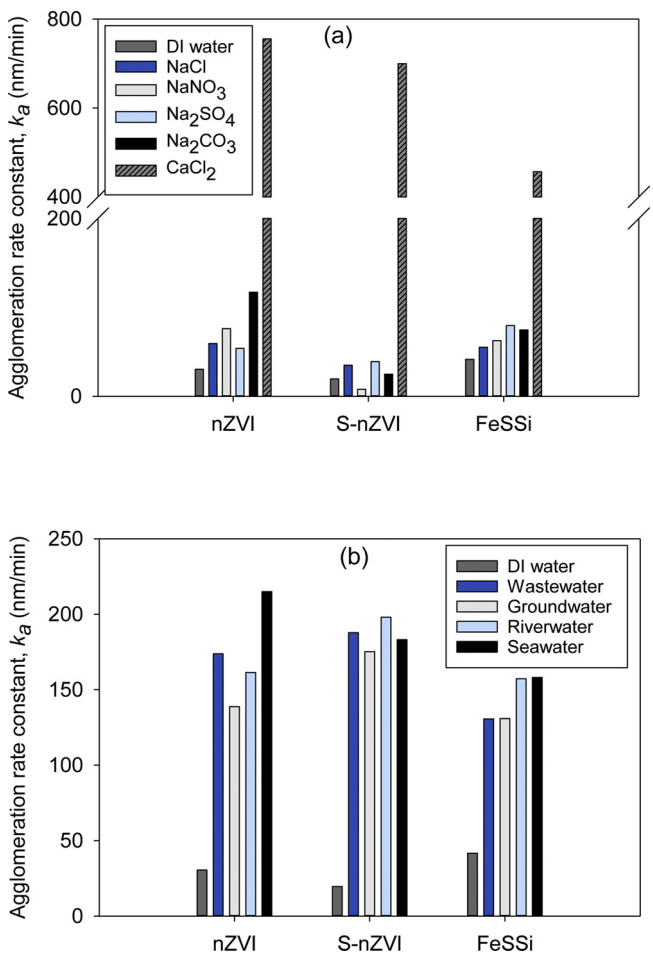

Fig. 3. Initial agglomeration rate constants of nZVI, S-nZVI, and FeSSi in (a) selected synthetic media, and (b) different water bodies and DI water.

(Fig. 3a). Of the three NPs, S-nZVI consistently had the lowest k_a in all the Na salts. The highest k_a for S-nZVI was observed in the presence of the divalent anion, SO_4^{2-} (39.0 nm/min); while the lowest k_a was found in the presence of NO_3- (7.91 nm/min). Like S-nZVI, FeSSi also had the highest k_a in the sulfate salt but the lowest k_a was observed in the presence of Cl-. Similar to the two sulfidated NPs, the highest k_a for nZVI in the Na salts was observed in the presence of a divalent anion, CO_3^{2-} (117.2 nm/min), but its k_a was similar in Cl- (59.5 nm/min) and SO_4^{2-} (54.0 nm/min). The impact of the different anions is mainly due to their interactions with the surface of the NPs, which may lead to changes in the surface charge (and thus electrostatic repulsion) of particles. In addition, common anions influence the transformations (corrosion) of nZVI differently (Su et al., 2018b; Pullin et al., 2017), which may impact the colloidal stability of the NPs. Although expected to be mostly similar, studies are needed to confirm the differential roles of common anions on the corrosion of sulfidated nZVI particles.

The fastest agglomeration was observed in the presence of Ca^{2+} due to the greater impact of the divalent cation on the electric double layer of the NPs. The initial hydrodynamic diameter of the three NPs was much larger in $CaCl_2$, and reached the micron scale within 2 min (Figure S2), similar to a previous report investigating the stability of nZVI in $CaCl_2$ (Song et al., 2017b). The k_a of nZVI, S-nZVI, and FeSSi increased from 59.5, 35.1, and 55.2 nm/min (respectively) in 10 mM NaCl to 755.4, 699.9, and 456.8 nm/min (respectively) in 10 mM $CaCl_2$. Thus, the application of the NPs in groundwater with high Ca^{2+} content may be limited due to rapid agglomeration. The mobility of the NPs in the subsurface is generally limited, but FeSSi, which had the lowest k_a in the presence of Ca^{2+}, may be more suitable for performing remediation in seawater-intruded aquifers, assuming the three particles have comparable removal performance. For the Na salts, k_a of nZVI was $Na_2CO_3 > NaNO_3 > Na_2SO_4 \approx NaCl$; that of S-nZVI was $Na_2SO_4 \approx NaCl > Na_2CO_3 > NaNO_3$; and that of FeSSi was $Na_2CO_3 \approx Na_2SO_4 > NaNO_3 \approx NaCl$. One implication of this result is that even if the three NPs have the same potential for remediating a pollutant, nZVI and FeSSi may not be as suitable as S-nZVI for performing remediation of contaminants in limestone-rich aquifers due to their higher tendency to agglomerate (under these conditions), which will lead to lower mobility.

3.2. Stability experiments in different water bodies

To better understand the stability of these NPs in the real environment, we also investigated the agglomeration kinetics of the NPs in groundwater, river water, wastewater, and sea water. The NPs agglomerated faster in the four water types obtained from the environment than in DI water (Fig. 3b), which is in agreement with our observation when individual salts were added to the NP suspensions (Fig. 3a). However, the k_a of the three NPs was much larger in the natural waters (130.6–215 nm/min) than all the Na salts (7.91–117.2 nm/min). In addition, the agglomeration kinetics observed in 10 mM $CaCl_2$ (456.8–755.4 nm/min) was much larger than in all the waters, including seawater (which has ~12 mM Ca and very high

concentrations of other cations like Na, Mg, and K (Conway et al., 2015)). The mechanism behind this trend needs in-depth investigation but one possible explanation may be the presence of anions and organic materials in seawater (but absent in $CaCl_2$ solution), which may bind with NPs and decrease k_a of NPs by electrosteric repulsion (Adeleye et al., 2016c).

S-nZVI was generally the most stable NP in the simple waters. In contrast, S-nZVI had the largest k_a in most of the natural waters (all except seawater) while the other sulfidated NP, FeSSi, had the lowest k_a in all the natural waters. Thus, silica seeding, in addition to sulfidation improves the colloidal stability of nZVI in natural waters. Also, this result emphasizes the need to perform experiments in conditions as close to the natural environment as possible for predicting the environmental implication of NPs.

3.3. Nanoparticle transport in sand columns

To compare the mobility of NPs in groundwater, saturated sand column studies were performed using synthetic groundwater. The Fe in the 51 PV effluent of nZVI, S-nZVI, and FeSSi accounted for 2.65 ± 0.81 %, 3.62 ± 0.54 %, and 3.07 ± 1.62 % of the total Fe added into column, respectively. This indicates that most of the NPs were retained in the columns; but the mean concentration of Fe in the effluent from columns with S-nZVI and FeSSi was slightly higher. As shown in Fig. 4, the bulk of the nZVI particles was deposited in the top layers of the saturated sand while sulfidation enhanced the mobility of the particles in the sand. In Layer 1 (top 2 cm of the soil), over 57 % of the total injected nZVI was retained while about 44 % of S-nZVI and FeSSi was detected in this layer ($p < 0.05$). This implies that sulfidation promoted the mobility of nZVI beyond the topmost soil surface. In Layer 2, the highest Fe content was detected in the column with FeSSi (30.7 %), followed by S-nZVI (25.5 %) and nZVI (18.3 %) ($p < 0.05$). In Layers 3 and 4, while the Fe content in the columns was between 10 % and 15 %, the S-nZVI column had a slightly higher Fe ($p > 0.05$). Overall, the mobility of the three NPs was S-nZVI > FeSSi > nZVI.

In addition, we continuously monitored the Fe concentration in effluent collected every 1.5 PVs while passing 51 PV of groundwater through the soil column after the injection of NPs. Much more FeSSi eluted than either S-nZVI or nZVI in the first 20 PV (Fig. 4b). Relatively lower spikes in Fe concentration were observed in the nZVI and S-nZVI columns around 24–30 PV s. However, S-nZVI had the highest elution in the last 10 PV. The earlier breakthrough of FeSSi likely resulted from size exclusion effects due to its larger size (200 nm) compared to the other two NPs (nZVI = 60 nm, and S-nZVI = 100 nm) (Babakhani, 2019). Size exclusion refers to the exclusion of particles from pores and stagnant domains that have smaller diameter or are less accessible, which allows larger particles to have higher mobility/breakthrough (Sirivithayapakorn and Keller, 2003). The smaller-sized S-nZVI probably did not remain within the main flow streams like FeSSi, thus, it had a slower breakthrough than FeSSi. The lack of clear breakthrough of nZVI emphasizes its strong retention in the topmost soil layer.

In addition to homoagglomeration between the NPs, heteroagglomeration between NPs and sand particles is also important in the transport of NPs in groundwater. The obtained result suggests that sulfidation decreased the attraction forces between the NPs and sand particles, enhancing their transport through the column. Thus, in addition to decreasing NP-NP agglomeration, sulfidation also decreases NP-sand agglomeration. Based on the groundwater pH of 6.5, nZVI (IEP = pH 7.5) was positively charged while S-nZVI (IEP = pH 5) and FeSSi (IEP = pH 5.5) were negatively charged. While electrostatic attraction was dominant between nZVI and sand (which is negatively charged) (Feriancikova and Xu, 2012), promoting heteroagglomeration; electrostatic repulsion was dominant between the sulfidated NPs and sand, which promoted their transport through the saturated column (Fazeli Sangani et al., 2019).

3.4. Chemical stability of metal-NPs composites

The chemical stability of the formed metal-NP composite is crucial for the long-term remediation of heavy metal pollution in groundwater. We investigated the long-term sequestration of Cu^{2+}, Zn^{2+}, Cd^{2+} and $Cr_2O_7^{2-}$ by the NPs, first in a synthetic groundwater (under anoxic condition), and thereafter in an oxic river water. As demonstrated in Fig. 5, all three NPs sequestered over 80 % of the metals/metallates in synthetic groundwater over 30 days. For $Cr_2O_7^{2-}$, S-nZVI had the highest removal capacity ($p < 0.05$, on Day 30), while the removal capacity of FeSSi was the lowest ($p < 0.05$, on Day 30). In contrast, S-nZVI had the lowest removal capacity for Cu^{2+} while FeSSi had the highest. After 10 days only 0.17 mg/L Cd^{2+} was detected in the supernatant of the reactor with S-nZVI, whereas 1.5 mg/L Cd^{2+} was measured in reactor dosed with nZVI. However, 5.6 %–14.8 % of the Cd^{2+} sequestered by all three NPs was remobilized between Days 10 and 30. For Zn^{2+}, all three NPs had a similar removal performance by Day 30 ($p > 0.05$).

These results imply that the three NPs can be potentially utilized to sequester metals from groundwater under anoxic conditions at circumneutral pH; but the efficiency of each NP is different for different metals. In addition, the different removal capacity of the three NPs for the metals reflects the differences in the pathways by which metals are immobilized onto iron-based NPs, including adsorption, co-precipitation and reduction (Su et al., 2015a; Zhang et al., 2013b; Su et al., 2016b, 2019). If the standard electrode potential of a metal is more positive than iron (Fe^{2+}/Fe°), then the metal ion could be reduced by the NPs following its adsorption and/or co-precipitation. Otherwise, the metal ion can only be adsorbed (or it can co-precipitate out from the solution). The differences in the density of adsorption sites on nZVI, S-nZVI, and FeSSi result in different adsorption capacity for metals. In terms of reduction, abundant Fe(0) in NPs and sufficient reaction time is favorable for metal removal while sulfidation does increase electron selectivity to targeted pollutants (Xu et al., 2020, 2019b; Li et al., 2018;

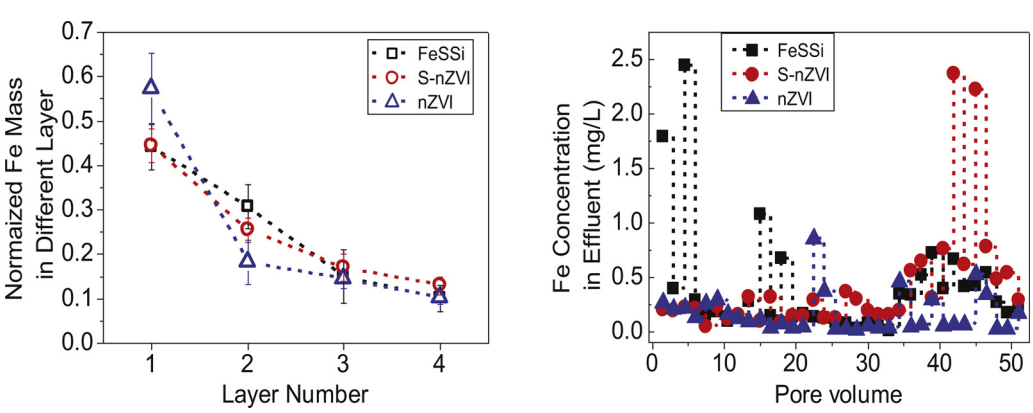

Fig. 4. (a) Distribution of NPs in column after 51 pore volumes (Layers 1, 2, 3, and 4 correspond to 0-2, 2-4, 4-6, and 6-9 cm from top of the column, respectively); (b) Fe concentration in effluent collected after 51 pore volumes at 1.5 pore volume interval (with synthetic groundwater as influent). (One-way analysis of variance (ANOVA) plus Fisher's LSD test were used to determine significant difference (defined as $p < 0.05$). There was significant difference in Fe concentrations collected from only Layers 1 and 2.

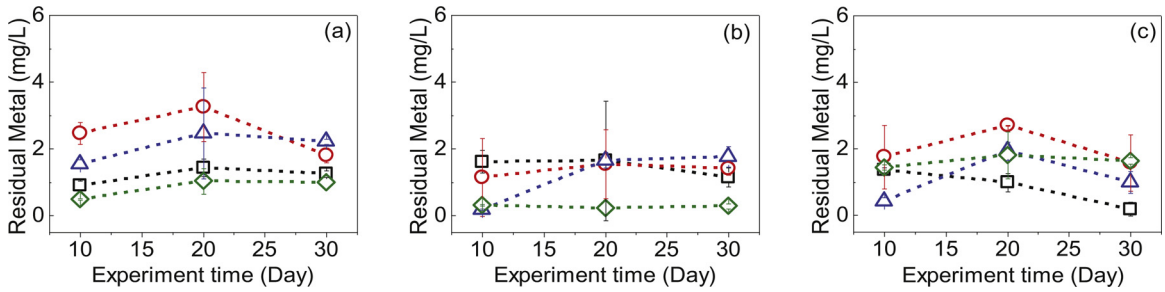

Fig. 5. Metal sequestration by (a) nZVI, (b) S-nZVI, and (c) FeSSi in synthetic groundwater (initial metal concentration = 10 mg/L; initial NP concentration = 0.5 g/L; = Cu^{2+}; = Zn^{2+}; = Cd^{2+}; and = $Cr_2O_7^{2-}$).

He et al., 2020).

To study the potential for the NP-sequestered metals/metallates to be remobilized if the composites were discharged with groundwater into a nearby surface water, additional studies were conducted: After 30 days of NPs-metals/metallates adsorption reaction in synthetic groundwater (under anoxic condition), the mixture (solids and liquid) was exposed to surface water under oxic conditions. Metals (contaminants and Fe) concentrations in the supernatant were thereafter monitored for 20 days. We observed considerable remobilization of most of the metals removed from synthetic groundwater immediately (day 0) after the discharge into river water (Fig. 6). However, most of the remobilized metals detected in supernatant were again sequestered within the 20-day study period (Fig. 6a). Similarly, dissolved Fe concentration increased right after exposure from groundwater to river water, and thereafter gradually decreased (Fig. 6b).

Of all the contaminant-NPs composites tested in river water, there was no remobilization of the $Cr_2O_7^{2-}$ previously adsorbed onto S-nZVI. Meanwhile, although was $Cr_2O_7^{2-}$ initially remobilized from nZVI and FeSSi into river water, it was no longer detected in the river water after 5 days. As for Cu^{2+}, nZVI demonstrated a slightly better re-adsorption performance in river water than S-nZVI and FeSSi after 20 days, although FeSSi was the best adsorbent for Cu^{2+} in synthetic groundwater. In contrast, the sulfidated particles, S-nZVI and FeSSi, showed a better removal performance than nZVI for Cd^{2+} and Zn^{2+} in river water. In fact, remobilization of Cd^{2+} and Zn^{2+} occurred in the nZVI system. This is in agreement with previous studies that have shown lower removal performance of Cd^{2+} and Zn^{2+} by nZVI (Su et al., 2015a, 2019; Adeleye et al., 2016d; Li et al., 2014). The concentration of Fe in the nZVI treatment increased simultaneously with that of Cd^{2+} and Zn^{2+}, which suggests that the metal-nZVI composites formed with Cd^{2+} and Zn^{2+} are not very chemically stable (compared to those formed with the sulfidated NPs) (Fig. 6b).

Our result suggests that the dissolution of metal-NP composites in the river water (where there is undersaturation with respect to the nanoparticles/nanocomposites) caused an initial increase in metal concentrations; and the likely precipitation of dissolved Fe in the water (that is, the formation of iron hydroxides due to the presence of dissolved oxygen, Figure S4) likely caused a re-sequestration of the metal contaminants. Notedly, a few chain-like structures were still observed in the S-nZVI reaction system (but not in nZVI reaction system, Figure S4), which is in line with the low dissolved Fe concentration observed in S-nZVI reaction system compared to that in the nZVI reaction system. This indicates that S-nZVI is more stable (even in oxic conditions), which contributes to the high chemical stability of metal-S-nZVI hybrids. This is in agreement with a previous study (Song et al., 2017b) in which we found that nZVI reacts much faster with dissolved oxygen than S-nZVI, leading to more dissolution of nZVI. Additional studies are needed to confirm the crystal structure of the precipitated Fe as well as the mechanism of re-sequestration of the metals, which are beyond the scope of this work. It should be noted that in open waters where the contaminants and nanoparticles are not confined to a limited space, remobilized metals may not be easily re-sequestered. In this respect, S-

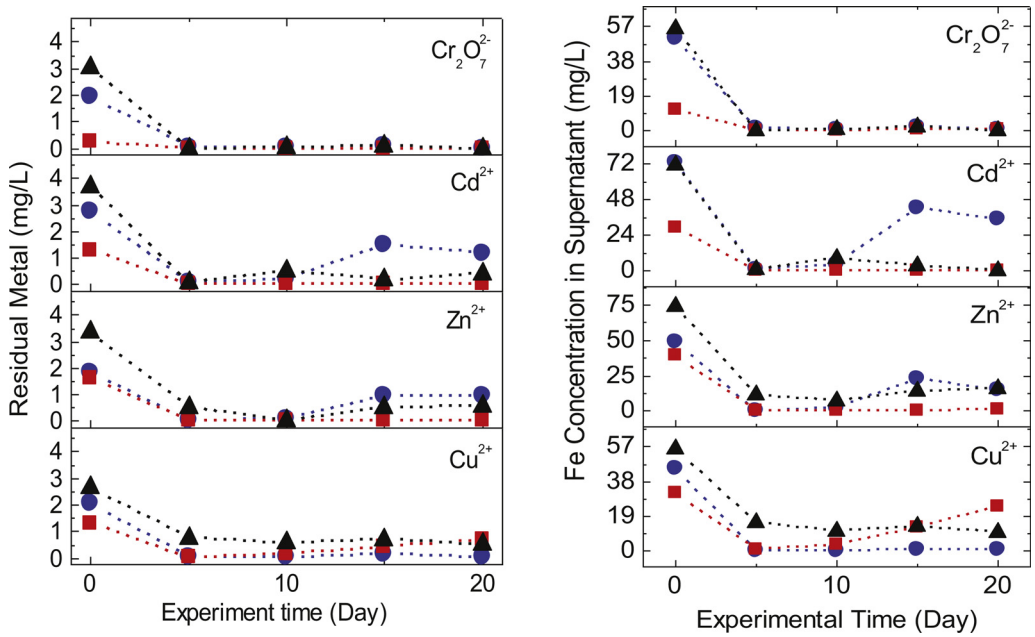

Fig. 6. Concentration of (a) residual metal and (b) dissolved Fe in supernatant after metal-NPs mixtures were exposed to river water (initial metal concentration = 3.3 mg/L; initial NP concentration = 0.167 g/L; = nZVI; = S-nZVI; and = FeSSi).

nZVI (with lower dissolution rate in river water) is likely more favorable for metal removal than nZVI and FeSSi.

Overall, even for metal ions that could be reduced by Fe(0) (such as Cu^{2+} and $Cr_2O_7^{2-}$) the adsorbed/co-precipitated metals on nZVI/S-nZVI/FeSSi could potentially be released back to water again under some conditions (such as oxic or acidic conditions) if they have not yet been completely reduced to zero valent metals. For those with more negative standard electrode potential than Fe^{2+}/Fe^0, such as Zn^{2+}/Zn^0, the chemical stability of metal-nZVI composites might be even weaker, although sulfidation can enhance the stability of these composites. Therefore, careful investigation of water quality and hydrology before injection, and constant monitoring (for metal remobilization, metal-NP composite transport, etc.) thereafter, are necessary for groundwater metal contamination treatment.

4. Conclusion

Sulfidation improved the colloidal stability of nZVI in both artificial and natural waters, although pristine nZVI was more colloidally stable in acidic condition. We also found evidence that sulfidation improved the mobility of nZVI in the sand column study. The amount of Fe in the effluent increased by 16–37 % upon the sulfidation of nZVI while much more Fe was transported below the top layer of the sand column. The three NPs tested, nZVI, S-nZVI, and FeSSi, sequestered over 80 % of metal ions from synthetic groundwater over a 30-day period with S-nZVI performing slightly better than nZVI. When the metal-NP composites were thereafter released into a river water (to simulate discharge with groundwater into a water body), there was a spike in dissolved metal concentration, due to dissolution of the metal-NP composites (leading to remobilization of the sequestered metal contaminants). Overall, the S-nZVI composites exhibited the highest chemical stability upon release into river water, as shown by the lowest amounts of dissolved metals and Fe. While sulfidation of nZVI to S-nZVI improves its colloidal stability, mobility, metal removal performance and chemical stability of metal-NP composites in the subsurface, it is of great importance to monitor the fate and transport of the composites since metals could be remobilized under certain conditions.

CRediT authorship contribution statement

Yiming Su: Conceptualization, Methodology, Investigation, Data curation, Writing - original draft, Writing - review & editing. **David Jassby:** Supervision, Resources, Writing - review & editing. **Yalei Zhang:** Supervision, Funding acquisition, Writing - review & editing. **Arturo A. Keller:** Supervision, Funding acquisition, Writing - review & editing. **Adeyemi S. Adeleye:** Conceptualization, Methodology, Investigation, Validation, Data curation, Writing - original draft, Writing - review & editing, Resources, Project administration.

Declaration of Competing Interest

The authors declare that they have no known competing financial interests or personal relationships that could have appeared to influence the work reported in this paper.

Acknowledgement

This material is based upon work supported by the National Natural Science Foundation of China (NSFC, NO. 21707103); the National Science Foundation (NSF) and the Environmental Protection Agency (EPA) under Cooperative Agreement Number DBI 0830117. Any opinions, findings, and conclusions or recommendations expressed in this material are those of the authors and do not necessarily reflect the views of NSF or EPA. This work has not been subjected to EPA review and no official endorsement should be inferred. We also acknowledge the lab assistance of Paige Rutten and Edward Hadeler.

Appendix A. Supplementary data

Supplementary material related to this article can be found, in the online version, at doi:https://doi.org/10.1016/j.jhazmat.2020.122691.

References

Adeleye, A.S., Keller, A.A., 2016. Interactions between algal extracellular polymeric substances and commercial TiO 2 nanoparticles in aqueous media. Environ. Sci. Technol. 50, 12258–12265. https://doi.org/10.1021/acs.est.6b03684.

Adeleye, A.S., Keller, A.A., Miller, R.J., Lenihan, H.S., 2013. Persistence of commercial nanoscaled zero-valent iron (nZVI) and by-products. J. Nanopart. Res. 15. https://doi.org/10.1007/s11051-013-1418-7.

Adeleye, A.S., Conway, J.R., Garner, K., Huang, Y., Su, Y., Keller, A.A., 2016a. Engineered nanomaterials for water treatment and remediation: costs, benefits, and applicability. Chem. Eng. J. 286, 640–662. https://doi.org/10.1016/j.cej.2015.10.105.

Adeleye, A.S., Oranu, E.A., Tao, M., Keller, A.A., 2016b. Release and detection of nanosized copper from a commercial antifouling paint. Water Res. 102, 374–382. https://doi.org/10.1016/j.watres.2016.06.056.

Adeleye, A.S., Stevenson, L.M., Su, Y., Nisbet, R.M., Zhang, Y., Keller, A.A., 2016c. Influence of phytoplankton on fate and effects of modified zerovalent Iron nanoparticles. Environ. Sci. Technol. 50, 5597–5605. https://doi.org/10.1021/acs.est.5b06251.

Adeleye, A.S., Conway, J.R., Garner, K., Huang, Y., Su, Y., Keller, A.A., 2016d. Engineered nanomaterials for water treatment and remediation: costs, benefits, and applicability. Chem. Eng. J. 286. https://doi.org/10.1016/j.cej.2015.10.105.

Babakhani, P., 2019. The impact of nanoparticle aggregation on their size exclusion during transport in porous media: one- and three-dimensional modelling investigations. Sci. Rep. https://doi.org/10.1038/s41598-019-50493-6.

Bello, A., Leiviskä, T., Zhang, R., Tanskanen, J., Maziarz, P., Matusik, J., Bhatnagar, A., 2019. Synthesis of zerovalent iron from water treatment residue as a conjugate with kaolin and its application for vanadium removal. J. Hazard. Mater. https://doi.org/10.1016/j.jhazmat.2019.04.056.

Chang, Q., Lin, W., chi Ying, W., 2010. Preparation of iron-impregnated granular activated carbon for arsenic removal from drinking water. J. Hazard. Mater. https://doi.org/10.1016/j.jhazmat.2010.08.066.

Chen, K.L., Elimelech, M., 2007. Influence of humic acid on the aggregation kinetics of fullerene (C60) nanoparticles in monovalent and divalent electrolyte solutions. J. Colloid Interface Sci. 309, 126–134. https://doi.org/10.1016/j.jcis.2007.01.074.

Chen, K.F., Li, S., Zhang, W.X., 2011. Renewable hydrogen generation by bimetallic zero valent iron nanoparticles. Chem. Eng. J. https://doi.org/10.1016/j.cej.2010.12.019.

Chowdhury, I., Hou, W.C., Goodwin, D., Henderson, M., Zepp, R.G., Bouchard, D., 2015. Sunlight affects aggregation and deposition of graphene oxide in the aquatic environment. Water Res. https://doi.org/10.1016/j.watres.2015.04.001.

Conway, J.R., Adeleye, A.S., Gardea-Torresdey, J., Keller, A.A., 2015. Aggregation, Dissolution, and Transformation of Copper Nanoparticles in Natural Waters. Environ. Sci. Technol. 49, 2749–2756. https://doi.org/10.1021/es504918q.

Fan, D., O'Brien Johnson, G., Tratnyek, P.G., Johnson, R.L., 2016. Sulfidation of nano zerovalent iron (nZVI) for improved selectivity during in-situ chemical reduction (ISCR). Environ. Sci. Technol. 50, 9558–9565. https://doi.org/10.1021/acs.est.6b02170.

Fan, D., Lan, Y., Tratnyek, P.G., Johnson, R.L., Filip, J., O'Carroll, D.M., Nunez Garcia, A., Agrawal, A., 2017a. Sulfidation of iron-based materials: a review of processes and implications for water treatment and remediation. Environ. Sci. Technol. https://doi.org/10.1021/acs.est.7b04177.

Fan, D., Lan, Y., Tratnyek, P.G., Johnson, R.L., Filip, J., O'Carroll, D.M., Nunez Garcia, A., Agrawal, A., 2017b. Sulfidation of iron-based materials: a review of processes and implications for water treatment and remediation. Environ. Sci. Technol. https://doi.org/10.1021/acs.est.7b04177. acs.est.7b04177.

Fazeli Sangani, M., Owens, G., Fotovat, A., 2019. Transport of engineered nanoparticles in soils and aquifers. Environ. Rev. https://doi.org/10.1139/er-2018-0022.

Feriancikova, L., Xu, S., 2012. Deposition and remobilization of graphene oxide within saturated sand packs. J. Hazard. Mater. https://doi.org/10.1016/j.jhazmat.2012.07.041.

He, Y.T., Wan, J., Tokunaga, T., 2008. Kinetic stability of hematite nanoparticles: the effect of particle sizes. J. Nanopart. Res. 10, 321–332. https://doi.org/10.1007/s11051-007-9255-1.

He, F., Zhao, D., Paul, C., 2010. Field assessment of carboxymethyl cellulose stabilized iron nanoparticles for in situ destruction of chlorinated solvents in source zones. Water Res. https://doi.org/10.1016/j.watres.2009.12.041.

He, F., Gong, L., Fan, D., Tratnyek, P.G., Lowry, G.V., 2020. Quantifying the efficiency and selectivity of organohalide dechlorination by zerovalent iron. Environ. Sci. Process. Impacts. https://doi.org/10.1039/C9EM00592G.

Jiemvarangkul, P., Zhang, W.X., Lien, H.L., 2011. Enhanced transport of polyelectrolyte stabilized nanoscale zero-valent iron (nZVI) in porous media. Chem. Eng. J. https://doi.org/10.1016/j.cej.2011.02.065.

Kadu, B.S., Chikate, R.C., 2013. NZVI based nanocomposites: role of noble metal and clay support on chemisorptive removal of Cr(VI). J. Environ. Chem. Eng. https://doi.org/10.1016/j.jece.2013.05.011.

Keller, A.A., Wang, H., Zhou, D., Lenihan, H.S., Cherr, G., Cardinale, B.J., Miller, R., Zhaoxia, J.I., 2010. Stability and aggregation of metal oxide nanoparticles in natural aqueous matrices. Environ. Sci. Technol. 44, 1962–1967. https://doi.org/10.1021/es902987d.

Lei, C., Sun, Y., Tsang, D.C.W., Lin, D., 2018. Environmental transformations and ecological effects of iron-based nanoparticles. Environ. Pollut. 232, 10–30. https://doi.

org/10.1016/j.envpol.2017.09.052.
Li, X.Q., Cao, J., Zhang, W.X., 2008. Stoichiometry of Cr(VI) immobilization using nanoscale zero valent iron (nZVI): a study with high-resolution X-ray photoelectron spectroscopy (HR-XPS). Ind. Eng. Chem. Res. 47, 2131–2139. https://doi.org/10.1021/ie061655x.
Li, S., Wang, W., Liu, Y., Xian Zhang, W., 2014. Zero-valent iron nanoparticles (nZVI) for the treatment of smelting wastewater: a pilot-scale demonstration. Chem. Eng. J. 254, 115–123. https://doi.org/10.1016/j.cej.2014.05.111.
Li, S., Wang, W., Liang, F., Zhang, W., 2016. Heavy metal removal using nanoscale zero-valent iron (nZVI): theory and application. J. Hazard. Mater. 1–9. https://doi.org/10.1016/j.jhazmat.2016.01.032.
Li, J., Zhang, X., Liu, M., Pan, B., Zhang, W., Shi, Z., Guan, X., 2018. Enhanced reactivity and Electron selectivity of sulfidated zerovalent Iron toward chromate under aerobic conditions. Environ. Sci. Technol. https://doi.org/10.1021/acs.est.7b06502.
Ling, L., Huang, X., Li, M., Zhang, W., 2017. Mapping the reactions in a single zero-valent Iron nanoparticle. Environ. Sci. Technol. 51, 14293–14300. https://doi.org/10.1021/acs.est.7b02233.
Ling, L., Tang, C., Zhang, W.X., 2018. Visualization of silver nanoparticle formation on nanoscale zero-valent Iron. Environ. Sci. Technol. Lett. https://doi.org/10.1021/acs.estlett.8b00259.
Liu, Y., Lowry, G.V., 2006. Effect of particle age (Fe0 content) and solution pH on NZVI reactivity: H2 evolution and TCE dechlorination. Environ. Sci. Technol. 40, 6085–6090. https://doi.org/10.1021/es060685o.
Liu, Y., Phenrat, T., Lowry, G.V., 2007. Effect of TCE concentration and dissolved groundwater solutes on NZVI-promoted TCE dechlorination and H2 evolution. Environ. Sci. Technol. 41, 7881–7887. https://doi.org/10.1021/es0711967.
Liu, J., Liu, A., xian Zhang, W., 2016. The influence of polyelectrolyte modification on nanoscale zero-valent iron (nZVI): aggregation, sedimentation, and reactivity with Ni (II) in water. Chem. Eng. J. https://doi.org/10.1016/j.cej.2016.05.132.
Mackenzie, K., Bleyl, S., Georgi, A., Kopinke, F.D., 2012. Carbo-iron - an Fe/AC composite - as alternative to nano-iron for groundwater treatment. Water Res. https://doi.org/10.1016/j.watres.2012.04.013.
Mangayayam, M., Dideriksen, K., Ceccato, M., Tobler, D.J., 2019. The structure of sulfidized zero-valent Iron by one-pot synthesis: impact on contaminant selectivity and long-term performance. Environ. Sci. Technol. https://doi.org/10.1021/acs.est.8b06480.
Middeldorp, P.J.M., Van Aalst, M.A., Rijnaarts, H.H.M., Stams, F.J.M., De Kreuk, H.F., Schraa, G., Bosma, T.N.P., 1998. Stimulation of reductive dechlorination for in situ bioremediation of a soil contaminated with chlorinated ethenes. Water Sci. Technol. https://doi.org/10.1016/S0273-1223(98)00240-6.
Mueller, N.C., Braun, J., Bruns, J., Černík, M., Rissing, P., Rickerby, D., Nowack, B., 2012. Application of nanoscale zero valent iron (NZVI) for groundwater remediation in Europe. Environ. Sci. Pollut. Res. https://doi.org/10.1007/s11356-011-0576-3.
na Shi, L., Lin, Y.M., Zhang, X., liang Chen, Z., 2011. Synthesis, characterization and kinetics of bentonite supported nZVI for the removal of Cr(VI) from aqueous solution. Chem. Eng. J. https://doi.org/10.1016/j.cej.2011.04.038.
Nunez Garcia, A., Boparai, H.K., de Boer, C.V., Chowdhury, A.I.A., Kocur, C.M.D., Austrins, L.M., Herrera, J., O'Carroll, D.M., 2020. Fate and transport of sulfidated nano zerovalent iron (S-nZVI): a field study. Water Res. 170, 115319. https://doi.org/10.1016/j.watres.2019.115319.
O'Carroll, D., Sleep, B., Krol, M., Boparai, H., Kocur, C., 2013. Nanoscale zero valent iron and bimetallic particles for contaminated site remediation. Adv. Water Resour. https://doi.org/10.1016/j.advwatres.2012.02.005.
Phenrat, T., Saleh, N., Sirk, K., Tilton, R.D., Lowry, G.V., 2007. Aggregation and sedimentation of aqueous nanoscale zerovalent iron dispersions. Environ. Sci. Technol. https://doi.org/10.1021/es061349a.
Phenrat, T., Saleh, N., Sirk, K., Kim, H.J., Tilton, R.D., Lowry, G.V., 2008. Stabilization of aqueous nanoscale zerovalent iron dispersions by anionic polyelectrolytes: adsorbed anionic polyelectrolyte layer properties and their effect on aggregation and sedimentation. J. Nanopart. Res. https://doi.org/10.1007/s11051-007-9315-6.
Pullin, H., Crane, R.A., Morgan, D.J., Scott, T.B., 2017. The effect of common groundwater anions on the aqueous corrosion of zero-valent iron nanoparticles and associated removal of aqueous copper and zinc. J. Environ. Chem. Eng. https://doi.org/10.1016/j.jece.2017.01.038.
Qian, D., Su, Y., Huang, Y., Chu, H., Zhou, X., Zhang, Y., 2018. Simultaneous molybdate (Mo(VI)) recovery and hazardous ions immobilization via nanoscale zerovalent iron. J. Hazard. Mater. 344, 698–706. https://doi.org/10.1016/j.jhazmat.2017.10.036.
Qin, H., Li, J., Yang, H., Pan, B., Zhang, W., Guan, X., 2017. Coupled effect of ferrous ion and oxygen on the electron selectivity of zerovalent Iron for selenate sequestration. Environ. Sci. Technol. https://doi.org/10.1021/acs.est.6b04832.
Raychoudhury, T., Naja, G., Ghoshal, S., 2010. Assessment of transport of two polyelectrolyte-stabilized zero-valent iron nanoparticles in porous media. J. Contam. Hydrol. https://doi.org/10.1016/j.jconhyd.2010.09.005.
Roehrdanz, P.R., Feraud, M., Lee, D.G., Means, J.C., Snyder, S.A., Holden, P.A., 2017. Spatial models of sewer pipe leakage predict the occurrence of wastewater indicators in shallow urban groundwater. Environ. Sci. Technol. https://doi.org/10.1021/acs.est.6b05015.
Shao, Q., Xu, C., Wang, Y., Huang, S., Zhang, B., Huang, L., Fan, D., Tratnyek, P.G., 2018. Dynamic interactions between sulfidated zerovalent iron and dissolved oxygen: mechanistic insights for enhanced chromate removal. Water Res. 135, 322–330. https://doi.org/10.1016/j.watres.2018.02.030.
Shi, D., Zhu, G., Zhang, X., Zhang, X., Li, X., Fan, J., 2019. Ultra-small and recyclable zero-valent iron nanoclusters for rapid and highly efficient catalytic reduction of: P-nitrophenol in water. Nanoscale. https://doi.org/10.1039/c8nr08302a.
Sirivithayapakorn, S., Keller, A., 2003. Transport of colloids in saturated porous media: a pore-scale observation of the size exclusion effect and colloid acceleration. Water Resour. Res. https://doi.org/10.1029/2002WR001583.
Song, S., Su, Y., Adeleye, A.S., Zhang, Y., Zhou, X., 2017a. Optimal design and characterization of sulfide-modified nanoscale zerovalent iron for diclofenac removal. Appl. Catal. B Environ. 201, 211–220. https://doi.org/10.1016/j.apcatb.2016.07.055.
Song, S., Su, Y., Adeleye, A.S., Zhang, Y., Zhou, X., 2017b. Optimal design and characterization of sulfide-modified nanoscale zerovalent iron for diclofenac removal. Appl. Catal. B Environ. 201, 211–220. https://doi.org/10.1016/j.apcatb.2016.07.055.
Su, Y., Adeleye, A.S., Zhou, X., Dai, C., Zhang, W., Keller, A.A., Zhang, Y., 2014a. Effects of nitrate on the treatment of lead contaminated groundwater by nanoscale zerovalent iron. J. Hazard. Mater. 280, 504–513. https://doi.org/10.1016/j.jhazmat.2014.08.040.
Su, Y., Adeleye, A.S., Huang, Y., Sun, X., Dai, C., Zhou, X., Zhang, Y., Keller, A.A., 2014b. Simultaneous removal of cadmium and nitrate in aqueous media by nanoscale zerovalent iron (nZVI) and Au doped nZVI particles. Water Res. 63, 102–111. https://doi.org/10.1016/j.watres.2014.06.008.
Su, Y., Adeleye, A.S., Keller, A.A., Huang, Y., Dai, C., Zhou, X., Zhang, Y., 2015a. Magnetic sulfide-modified nanoscale zerovalent iron (S-nZVI) for dissolved metal ion removal. Water Res. 74, 47–57. https://doi.org/10.1016/j.watres.2015.02.004.
Su, Y., Adeleye, A.S., Keller, A.A., Huang, Y., Dai, C., Zhou, X., Zhang, Y., 2015b. Magnetic sulfide-modified nanoscale zerovalent iron (S-nZVI) for dissolved metal ion removal. Water Res. 74, 47–57. https://doi.org/10.1016/j.watres.2015.02.004.
Su, Y., Adeleye, A.S., Huang, Y., Zhou, X., Keller, A.A., Zhang, Y., 2016a. Direct synthesis of novel and reactive sulfide-modified nano iron through nanoparticle seeding for improved cadmium-contaminated water treatment. Sci. Rep. 6, 24358. https://doi.org/10.1038/srep24358.
Su, Y., Adeleye, A.S., Huang, Y., Zhou, X., Keller, A.A., Zhang, Y., 2016b. Direct synthesis of novel and reactive sulfide-modified nano Iron through nanoparticle seeding for improved cadmium-contaminated water treatment. Sci. Rep. 6, 24358. https://doi.org/10.1038/srep24358.
Su, Y., Jassby, D., Song, S., Zhou, X., Zhao, H., Filip, J., Petala, E., Zhang, Y., 2018a. Enhanced oxidative and adsorptive removal of diclofenac in heterogeneous fenton-like reaction with sulfide modified nanoscale zerovalent Iron. Environ. Sci. Technol. 52, 6466–6475. https://doi.org/10.1021/acs.est.8b00231.
Su, Y., Qian, D., Adeleye, A.S., Zhang, J., Zhou, X., Jassby, D., Zhang, Y., 2018b. Impact of ageing on the fate of molybdate-zerovalent iron nanohybrid and its subsequent effect on cyanobacteria (Microcystis aeruginosa) growth in aqueous media. Water Res. 140, 135–147. https://doi.org/10.1016/j.watres.2018.04.037.
Su, Y., Lowry, G.V., Jassby, D., Zhang, Y., 2019. Sulfide-modified NZVI (S-NZVI): synthesis, characterization, and reactivity. In: Phenrat, T., Lowry, G.V. (Eds.), Nanoscale Zerovalent Iron Part. Environ. Restor., 1st ed. Springer International Publishing, Cham, pp. 359–386. https://doi.org/10.1007/978-3-319-95340-3_9.
Tang, J., Tang, L., Feng, H., Zeng, G., Dong, H., Zhang, C., Huang, B., Deng, Y., Wang, J., Zhou, Y., 2016. pH-dependent degradation of p-nitrophenol by sulfidated nanoscale zerovalent iron under aerobic or anoxic conditions. J. Hazard. Mater. 320, 581–590. https://doi.org/10.1016/j.jhazmat.2016.07.042.
Wang, X., Adeleye, A.S., Wang, H., Zhang, M., Liu, M., Wang, Y., Li, Y., Keller, A.A., 2018. Interactions between polybrominated diphenyl ethers (PBDEs) and TiO2 nanoparticle in artificial and natural waters. Water Res. https://doi.org/10.1016/j.watres.2018.09.019.
Xiang, Y., Xu, Z., Wei, Y., Zhou, Y., Yang, X., Yang, Y., Yang, J., Zhang, J., Luo, L., Zhou, Z., 2019. Carbon-based materials as adsorbent for antibiotics removal: mechanisms and influencing factors. J. Environ. Manage. 237, 128–138. https://doi.org/10.1016/j.jenvman.2019.02.068.
Xiang, Y., Yang, X., Xu, Z., Hu, W., Zhou, Y., Wan, Z., Yang, Y., Wei, Y., Yang, J., Tsang, D.C.W., 2020. Fabrication of sustainable manganese ferrite modified biochar from vinasse for enhanced adsorption of fluoroquinolone antibiotics: effects and mechanisms. Sci. Total Environ. 709, 136079. https://doi.org/10.1016/j.scitotenv.2019.136079.
Xu, J., Cao, Z., Zhou, H., Lou, Z., Wang, Y., Xu, X., Lowry, G.V., 2019a. Sulfur dose and sulfidation time affect reactivity and selectivity of post-sulfidized nanoscale zerovalent Iron. Environ. Sci. Technol. 53, 13344–13352. https://doi.org/10.1021/acs.est.9b04210.
Xu, J., Wang, Y., Weng, C., Bai, W., Jiao, Y., Kaegi, R., Lowry, G.V., 2019b. Reactivity, selectivity, and long-term performance of sulfidized nanoscale zerovalent iron with different properties. Environ. Sci. Technol. 53, 5936–5945. https://doi.org/10.1021/acs.est.9b00511.
Xu, J., Avellan, A., Li, H., Liu, X., Noël, V., Lou, Z., Wang, Y., Kaegi, R., Henkelman, G., Lowry, G.V., 2020. Sulfur loading and speciation control the hydrophobicity, Electron transfer, reactivity, and selectivity of sulfidized nanoscale zerovalent Iron. Adv. Mater., 1906910. https://doi.org/10.1002/adma.201906910.
Yu, C., Shao, J.C., Sun, W.J., Yu, X.N., 2018. Treatment of lead contaminated water using synthesized nano-iron supported with bentonite/graphene oxide. Arab. J. Chem. https://doi.org/10.1016/j.arabjc.2018.11.019.
Zhang, W.X., 2003. Nanoscale iron particles for environmental remediation: an overview. J. Nanopart. Res. https://doi.org/10.1023/A:1025520116015.
Zhang, Y., Su, Y., Zhou, X., Dai, C., Keller, A.A., 2013a. A new insight on the core-shell structure of zerovalent iron nanoparticles and its application for Pb(II) sequestration. J. Hazard. Mater. 263, 685–693. https://doi.org/10.1016/j.jhazmat.2013.10.031.
Zhang, Y., Su, Y., Zhou, X., Dai, C., Keller, A.A., 2013b. A new insight on the core-shell structure of zerovalent iron nanoparticles and its application for Pb(II) sequestration. J. Hazard. Mater. 263. https://doi.org/10.1016/j.jhazmat.2013.10.031.